



Thermally stable TiO₂ quantum dots embedded in SiO₂ foams: Characterization and photocatalytic H₂ evolution activity

Donglai Pan^{b,1}, Zhiya Han^{b,1}, Yingchun Miao^{a,*}, Dieqing Zhang^b, Guisheng Li^{b,*}

^a Faculty of Chemical and Environment Sciences, Qijiang Normal University, Qijiang 655000, China

^b Key Laboratory of Resource Chemistry of Ministry of Education, Shanghai Key Laboratory of Rare Earth Functional Materials, Shanghai Normal University, Shanghai 200234, China



ARTICLE INFO

Keywords:

Silica
Foam
TiO₂
Quantum dots
H₂ evolution

ABSTRACT

Highly dispersed and thermally stable TiO₂ quantum dots (TiO₂-QDs) were achieved in the pore channels of SiO₂ foams with large pore size (14–20 nm) via in-situ hydrolysis of Ti-alkoxide. Owing to the anchoring effect between TiO₂-QDs and the pore-wall of SiO₂ foam, both the TiO₂ phase transformation from anatase to rutile and the aggregation of TiO₂-QDs were effectively prohibited. The anatase TiO₂-QDs anchored on the surface of silica foams could be well maintained with a ultrafine crystal size (< 7.0 nm) even after high temperature (up to 1000 °C) calcination in air, suggesting a high thermal stability. The sample of TiO₂-QDs/SiO₂ photocatalysts (molar ratio of Ti/Si = 60%, 900 °C) still exhibited a high H₂ evolution rate (HER, 10399 μmol g⁻¹ h⁻¹) for reducing water with a quantum efficiency of 17.8% under UV light irradiation (λ = 365 nm), slightly lower than that of the sample treated at 500 °C. In the absence of the silica foam, the pure TiO₂ crystals calcined at 900 °C crystals nearly cannot exhibit an obvious HER value. Such excellent photocatalytic hydrogen evolution performance was ascribed to the short electron-transfer distance, high anatase crystallinity, uniform dispersity in silica foam, and excellent stability of the TiO₂-QDs. This proposed route offered an effective platform for fabricating highly active metal oxide QDs with high thermal stability, greatly prolonging the recyclability.

1. Introduction

Metal oxide semiconductors, such as TiO₂, ZnO, WO₃, and SnO₂, have been applied as photocatalysts for splitting water for green energy hydrogen production and degrading toxic pollutants [1–6]. Among the abundant semiconductor materials, TiO₂ is generally believed to be the most reliable materials for photocatalytic reactions due to their non-toxicity, low cost, physical and chemical stability, availability, and unique electronic and optical properties [7–9].

As is known to us all, in order to maximize photocatalytic activity, TiO₂ particles are always shaped to nanocrystals with small size, offering large number of active sites by unit mass [10–12]. Nevertheless, it has to be acknowledged that some problems still existed if TiO₂ crystals were shaped to quantum dots (QDs). At quantum size scale, the effective applications of QDs were hindered by two serious problems. One relies that ultrafine nanoparticles tended to agglomerate into large particles, resulting in low surface area, losing active sites, and poor catalytic performance [13–19]. On the other hand, the separation and recovery of these QDs-based catalysts are usually very difficult and energy consuming [20–24]. Finally, it should be also pointed out that

QDs even made from non-toxic materials may cause toxicity to the environmental [25–27]. For those reasons, it is highly required to explore an effective route for both using and stabilizing TiO₂ QDs as a strong photocatalyst.

To date, researchers prefer to utilize mesoporous materials as supports to load titania as photocatalysts [28,29]. It was proved that depositing titanium dioxides onto a large internal surface or incorporating Ti species into porous frameworks could be utilized to fabricate advanced functional materials via taking advantages of both TiO₂ (n-type semiconductor and active catalyst) and SiO₂ (large surface area and high thermal stability). Furthermore, some special properties, not found in single oxide alone, could be achieved owing to the synergetic effects [30,31]. Up to now, mesoporous SiO₂-based materials, such as SBA-15, were usually chosen to immobilize TiO₂ crystals. However, the loaded percentage of Ti/Si molar ratio was very limited and most of the TiO₂ crystal grains were located outside of the pore channels owing to the fast hydrolysis of TiO₂ precursors [32–35]. Actually, the active species of TiO₂ crystals cannot be well protected by silica, most of them still suffered serious aggregation under high temperature calcination. Silica foams, with continuous 3D pore structure connected by window,

* Corresponding authors.

E-mail addresses: miaoyingchun1979@126.com (Y. Miao), liguisheng@shnu.edu.cn (G. Li).

¹ Equal contribution.

exhibited a larger pore size (> 20 nm) and higher hydrothermal stability compared to other mesoporous silica materials (SBA-15, MCM41, and etc.). Thus, it could be proved one of the most promising supports for immobilizing QDs-based photocatalysts [36].

In the present work, TiO_2 QDs were highly uniformly embedded in the framework of 3D silica foams via precisely controlling the hydrolyzing titanium precursor (Ti-alkoxide) in the internal channel of the silica foams. The as-synthesized TiO_2 -QDs/ SiO_2 composites possessed an excellent thermal stability (up to 1000 °C) and high photocatalytic activity for H_2 evolution owing to its large surface area, short electron-transfer distance, and high crystalline degree of anatase. The 3D windows opened SiO_2 foams supplied an effective nanosized reactor (pore channels) to allow the hydrolysis of titanium precursor in the channels of the silica foam. Compared to 2D mesoporous silica (SBA-15), such SiO_2 foam could greatly inhibit the growth of crystal size of TiO_2 grains and the phase transformation from anatase to rutile phase. This work also supplied an effective route for fabricating QDs-based functional materials with high thermal stability to be applied in solar cells, high temperature catalysis with high activity and long recyclability.

2. Experimental section

2.1. Materials

All chemicals were used as received without further treatment. Pluronic P123 (Mw = 5800, $\text{HO}(\text{CH}_2\text{CH}_2\text{O})_{20}-(\text{CH}_2\text{CHCH}_3\text{O})_{70}(\text{CH}_2\text{CH}_2\text{O})_{20}\text{H}$, $\text{EO}_{20}\text{PO}_{70}\text{EO}_{20}$, abbreviated as P123) was purchased from Sigma-Aldrich Co., Ltd., USA. Tetrabutyl titanate (TBT, $(\text{C}_4\text{H}_9\text{O})_4\text{Ti}$), 1,3,5-trimethylbenzene (TMB), NH_4F and Tetraethoxysilane (TEOS, $\text{CH}_3\text{CH}_2\text{OSi}(\text{OCH}_2\text{CH}_3)_3$) were obtained from Shanghai Aladdin Co., Ltd., China. Methanol and ethanol was supplied from Shanghai Jingchun Chemical Reagent Co. Ltd., Doubly distilled water was used for all synthesis and treatment processes.

2.2. Synthesis of SiO_2 foams

The SiO_2 foams was prepared based on the reported procedure [37,38]. P123 was used as a structure directing agent, and 1,3,5-trimethylbenzene (TMB) was used as an organic co-solvent. In a typical preparation process, 2.0 g of P123 was dissolved in 75 mL of aqueous HCl (1.6 M) under vigorous stirring at 40 °C. 23.0 mg of NH_4F and 2.0 g of TMB were added to the above solution, while keeping stirring for 45 min. To the as-formed solution, 4.4 g of TEOS was introduced. After being stirred for 20 h at 40 °C, a cloudy mixture was obtained and further transferred into a Teflon-lined steel autoclave, which was kept in an oven at 100 °C for 24 h. After cooling to room temperature, the precipitate in the bottom of Teflon vessel was collected, filtered, thoroughly washed with water to remove the remained chemicals and dried at room temperature with the formation of silica. The as-made silica was calcined at 500 °C for 8 h in air to produce SiO_2 foams to be used in the next experiment process.

2.3. Embedding TiO_2 -QDs in SiO_2 foams (TiO_2 -QDs/ SiO_2)

The sample of TiO_2 -QDs/ SiO_2 weas prepared by the hydrolysis of tetrabutyl titanate (TBT) in pore of the SiO_2 foams. In a typical procedure, calculated amount of TBT was dissolved in 70 mL ethanol under stirring with the formation of transparent solution. Then, 0.5 g SiO_2 foam was added to the above solution. This mixture solution was kept with vigorous stirring for 1 to allow the TBT molecules to be adsorbed in the channels of the SiO_2 foams channels. For initializing the hydrolysis of TBT molecules, D.I. water was dropped into the above solution slowly (2–3 drops/min). Vigorous stirring was kept for 2 h for making sure the completed hydrolysis of TBT. The as-obtained solid product was recovered by filtration, washed with ethanol to remove any unanchored titanium species, dried 80 °C overnight and calcined in air at

500 °C–1000 °C for 3 h. The calcined TiO_2 -QDs/ SiO_2 samples were designated as $\text{Ti/Si-x \%}-\text{T}$, where x % was the molar ratio of Ti:Si and T was the calcination temperature value. For better comparison, SBA-15 and commercial SiO_2 nanospheres was also utilized as supporter for loading TiO_2 species (named as $\text{TiO}_2/\text{SBA-15-x \%}-\text{T}$ and $\text{TiO}_2/\text{commercial SiO}_2-\text{x \%}-\text{T}$) while keeping other conditions unchanged. Pure TiO_2 was also synthesized in the absence of SiO_2 foams. It was named as TiO_2-T . The commercial TiO_2 (P25) was used as a reference.

2.4. Characterization

The crystallographic information of the samples was determined by X-ray diffraction (XRD, D/MAX-2000 with $\text{Cu K}\alpha 1$ irradiation). The morphology of the products were investigated by transmission electronic micrograph (TEM, JEM-2010, operated at 200 kV). BET surface area, pore volume and average pore diameter of TiO_2 / SiO_2 photocatalysts were measured by N_2 phys-isorption at –196 °C using TriStar II 3020 system. On the basis of the adsorption branches of N_2 sorption isotherms, the Brunauer-Emmett-Teller (BET) method was used to calculate the specific surface area (S_{BET}) and the Barrett-Joyner-Halenda (BJH) model was used to calculate pore volume (VP), and the pore size distribution. The FT-IR spectra were obtained on a Fourier transform infrared spectrometer (Bruker Equinox 55) using KBr pellets. UV-vis diffuse reflectance spectra (DRS) were obtained using a scan UV-vis spectrophotometer (DRS, MC-2530) equipped with an integrating sphere assembly, while BaSO_4 was used as a reference. The X-ray photoelectron spectroscopy (XPS) analysis was performed on a Perkin-Elmer PHI 5000C. All the binding energies were calibrated by using the contaminant carbon (C1s = 284.6 eV) as a reference.

2.5. Photocatalytic H_2 evolution activity

The photocatalytic H_2 -production experiments were performed in a 100 mL Pyrex flask at ambient temperature and atmospheric pressure, and a three-openings of flask was sealed with silicone rubber septum. In a typical photocatalytic experiment, 50.0 mg of TiO_2 / SiO_2 composite photocatalyst was suspended in 80.0 mL of aqueous solution containing methanol (25.0 V%) as sacrificial agents for trapping holes. Proper amount of H_2PtCl_6 aqueous solution was added in the above solution, Herein, 1.0 wt.% Pt, as a co-catalyst, was *in-suit* reduced during the photocatalytic hydrogen evolution reaction. Prior to light irradiation, the suspension of the photocatalyst was dispersed in an ultrasonic bath for 10 min. Then, the reactor was bubbled with nitrogen for 30 min to completely remove the dissolved oxygen and ensured that the reactor was in an anaerobic condition. A continuous magnetic stirrer was applied at the bottom of the reactor in order to keep the photocatalyst particles in suspension status during the whole experiment. 0.5 mL of gas was sampled intermittently through the septum after 1 h irradiation, and hydrogen was analyzed by gas chromatograph (GC9800, Shanghai Ke Chuang Chromatograph Instruments Co. Ltd, China, TCD, with nitrogen as a carrier gas and 5 Å molecular sieve column). All glassware was carefully rinsed with deionized water prior to use. The apparent quantum efficiency (QE) was measured under the same photocatalytic reaction conditions. Four low power UV-LEDs (3 W, 365 nm) (Shenzhen LAMPLIC Science Co. Ltd, China), which were positioned 1.0 cm away from the reactor in four different directions, were used as light sources to trigger the photocatalytic reaction. The focused intensity and areas on the flask for each UV-LED was ca. 80.0 mw cm^{-2} and 1.0 cm^2 , respectively. The QE was measured and calculated according to Eq. (1):

$$\begin{aligned} \text{QE} [\%] &= \frac{\text{number of reacted electrons}}{\text{number of incident photons}} \times 100 \\ &= \frac{\text{number of evolved H}_2\text{molecules} \times 2}{\text{number of incident photons}} \times 100 \end{aligned} \quad (1)$$

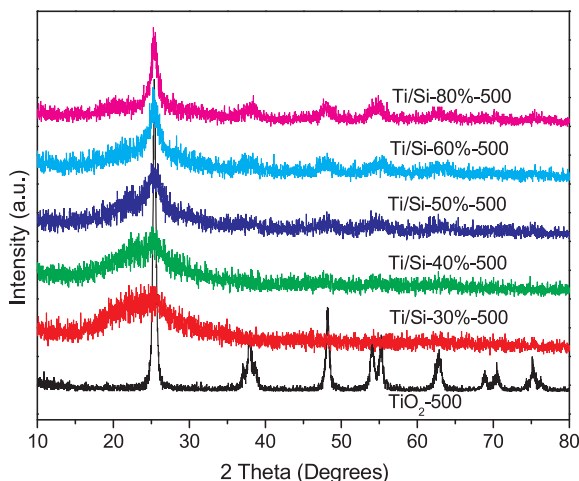


Fig. 1. XRD patterns of the pure TiO₂ and TiO₂/SiO₂ with various TiO₂ concentrations calcined at 500 °C.

2.6. Photocatalytic degradation of 4-CP

The photocatalytic degradation of p-Chloroaniline (4-CP) in an aqueous solution was evaluated under 300 W Xe lamp irradiation. 50.0 mg catalyst was added to 100 mL 4-CP (10 ppm) solution. Before light irradiation, the suspension was stirred for 120 min in the dark to achieve the adsorption-desorption equilibrium between 4-CP and the photocatalysts. During the photocatalytic reaction, 4 mL suspension was sampled from the solution, and the photocatalyst was removed by a filter. The concentration of 4-CP was analyzed by UV-vis spectrophotometer according to its absorbance at 279 nm.

3. Results and discussion

The Wide-angle XRD patterns of the pure TiO₂ and TiO₂ supported on SiO₂ foams with various TiO₂ concentration (30–80 %) calcined at 500 °C were shown in Fig. 1. To the case of the pure TiO₂ calcined at 500 °C (TiO₂-500), a typical of anatase TiO₂ crystalline phase was observed [37,38]. The average crystal size of TiO₂-500 was estimated to be about 16.4 nm based on the half-width of (101) peak using the Scherrer formula (listed in Table 1) [13]. Upon introducing SiO₂ foams for loading TiO₂, it was found that the patterns of the TiO₂-QDs/SiO₂ samples exhibited a typical broad diffraction peak centered at 2θ of 25.3° (attributed to the typically characteristic peaks of anatase TiO₂ crystalline TiO₂). Nearly no clear characteristic peaks of amorphous silica were observed in the XRD patterns of the TiO₂/SiO₂ samples. The relatively low diffraction intensity of SiO₂ at 22.0° could be shielded by the main peak of anatase TiO₂ crystalline at 25.3°. Nevertheless, such

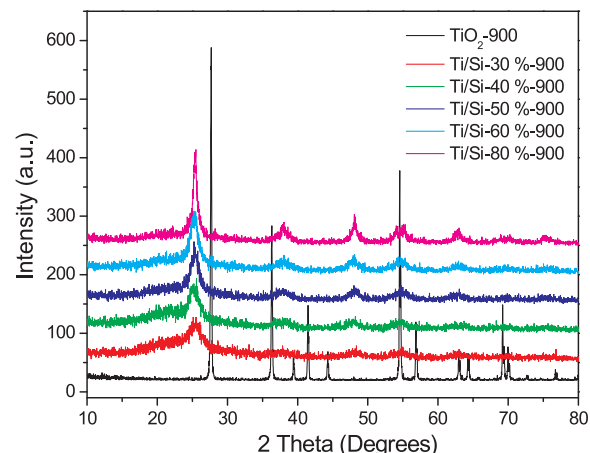


Fig. 2. XRD patterns of TiO₂/SiO₂ samples with different TiO₂ content and pure TiO₂ calcined at 900 °C.

broad (101) reflection peaks were slightly narrowed with improved intensity upon increasing the loaded TiO₂ content. This is because more anatase TiO₂ grains were formed on the surface of the SiO₂ foams. Meanwhile, it could be noticed that the average crystal size of anatase TiO₂ was greatly decreased to 2.1 nm in the presence of SiO₂ foam for the Ti/Si-30%-500 sample even after 3 h calcination at 500 °C. This suggested that the SiO₂ foams could effectively inhibit the crystal grain growth. Such ultrafine crystal grain size can be maintained to be about 6.8 nm even increasing the loaded TiO₂ amount to 80% Ti/Si ratio (Ti/Si-80%-500). Based on the above results, it was reasonable that ultrafine anatase TiO₂ QDs with an average crystal ranging from 2.1 nm to 6.8 nm could be fabricated and embedded in the framework of SiO₂ foams under high temperature calcination.

To investigate the thermal stability of the as-obtained TiO₂/SiO₂ composites, those samples were further calcined at 900 °C in air. As shown in Fig. 2, the pure anatase TiO₂ was transformed to rutile phase completely for the TiO₂-900 sample after calcination at 900 °C. The crystal grain size suffered a serious aggregation, with the formation of a large size of 42.6 nm (see Table 1). In the presence of the SiO₂ foam, the anatase phase of the TiO₂ QDS can be well maintained even being calcined at 900 °C, though the typical main anatase peak (101) of anatase phase was enhanced with a narrowed half-width of (101) peak. It was surprising that the crystal size of these embedded TiO₂-QDs can be still kept below 6.0 nm with high crystallization degree of anatase in the presence of a low Ti/Si molar ratio (< 60%). Actually, such well crystallized anatase TiO₂ with small size are highly required for photocatalysis process. As known, high anatase crystalline phase is favourable for enhancing the light driven activity [39,40] and the ultrafine crystal size may shorten the electron-transfer distance, thus more

Table 1

Textural properties and average crystal size of pure TiO₂ crystals (calculated from XRD patterns) and embedded in SiO₂ foams calcined at various temperatures.

samples	BET surface area (m ² /g)	structure	pore volume (cm ³ /g)	pore size (nm)	average crystal size (nm)
SiO ₂	612	–	2.16	14.1	–
Ti/Si-30 %-500	435	Anatase	1.46	13.9	2.1
Ti/Si-40 %-500	422	Anatase	1.21	11.1	2.3
Ti/Si-50 %-500	414	Anatase	1.18	10.9	3.6
Ti/Si-60 %-500	410	Anatase	0.756	9.41	4.1
Ti/Si-80 %-500	301	Anatase	0.671	6.57	6.8
TiO ₂ -500	14.3	Anatase	0.0247	6.91	16.4
Ti/Si-30 %-900	365	Anatase	1.20	17.1	3.2
Ti/Si-40 %-900	310	Anatase	1.03	11.3	4.4
Ti/Si-50 %-900	262	Anatase	0.921	12.1	5.8
Ti/Si-60 %-900	251	Anatase	0.874	13.7	6.3
Ti/Si-80 %-900	200	Anatase	0.688	13.7	9.9
TiO ₂ -900	–	Rutile	–	–	42.6

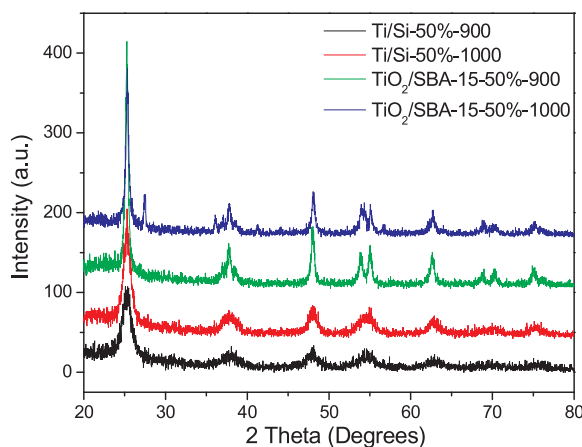


Fig. 3. XRD patterns of $\text{TiO}_2/\text{SiO}_2$ (Ti/Si molar ratio = 50%) samples calcined at 900 and 1000 °C via choosing silica foam and SBA-15 as supporters.

electrons in the body of TiO_2 may transfer to the surface, contributing a high electron-hole separation efficiency [41,42]. To further illustrate the promotion effect of the 3D silica foam on the thermal stability of the $\text{TiO}_2/\text{SiO}_2$ composites, a typical 2D silica (SBA-15) [43] was also utilized to load TiO_2 for comparison. As the calcination temperature was further increased to 1000 °C, the TiO_2 -QDs in the sample of Ti/Si-50%-1000 can be still maintained in the form of anatase phase with an average size of 6.1 nm calcined from the XRD results (Fig. 3). However, the TiO_2 grains supported by SBA-15 suffered both a phase-transform from anatase to rutile and a serious aggregation (average size = 17.6 nm). These results indicated that the 3D silica foam with large pore size could significantly inhibit the phase formation from anatase to rutile and the growth of TiO_2 crystal grain owing to its 3D large pore structures.

The porous structure and BET surface areas of the prepared TiO_2 -QDs/ SiO_2 composites were investigated using nitrogen adsorption-desorption. As shown in Fig. 4a, the sample of pure SiO_2 (calcined at 500 °C) exhibited an isotherm of typical type IV with a H1 hysteresis loop due to the capillary condensation steps at relative pressure of $0.6 < P/P_0 < 1.0$, which is characteristic of a mesoporous material according to IUPAC classification [44–47]. It was found that the H1 hysteresis loop can be well maintained upon loading TiO_2 -QDs, though the adsorbed amount of N_2 was decreased. Such a decrease of N_2 adsorption for these TiO_2 -QDs/ SiO_2 samples is reasonable, considering the formation of TiO_2 -QDs inside the large pores of the SiO_2 foams. The BET specific area, pore volumes and the pore size of the as-obtained samples were summarized in Table 1. It can be seen that loading TiO_2 -QDs resulted in a decrease of both BET surface area and pore volume compared to the pure SiO_2 foam. Nevertheless, it should be pointed out that these TiO_2 -QDs/ SiO_2 samples possessed a large surface area. For example, Ti/Si-50%-500 exhibited a surface area of $414 \text{ m}^2/\text{g}$, about 29 times of that ($14.3 \text{ m}^2/\text{g}$) of the TiO_2 nanoparticles calcined at 500 °C. We also noted that, in the presence of low concentration TiO_2 species (molar ratio of Ti/Si < 50%), just a slight decrease of pore volume was observed, suggesting that the pores in the silica foam were not blocked by the TiO_2 -QDs. These TiO_2 -QDs were uniformly dispersed on the pore wall of the SiO_2 foams. Thus, it can be concluded that such 3D mesoporous channels of SiO_2 foams may well control the size of TiO_2 -QDs limited in the pore channels. However, the pore volume was greatly decreased when the loaded Ti/Si molar ratio was higher than 60%. It indicated that excess TiO_2 species would destroy the pore structure of the SiO_2 foams, resulting in low pore volumes. This was in good agreement with previous observations of $\text{TiO}_2/\text{SiO}_2$ [48–52].

From Fig. 4b, it can be found that the mesoporous structures of the TiO_2 -QDs/ SiO_2 could be well maintained even after calcination at 900 °C. However, it should be pointed out the decrease percentages of

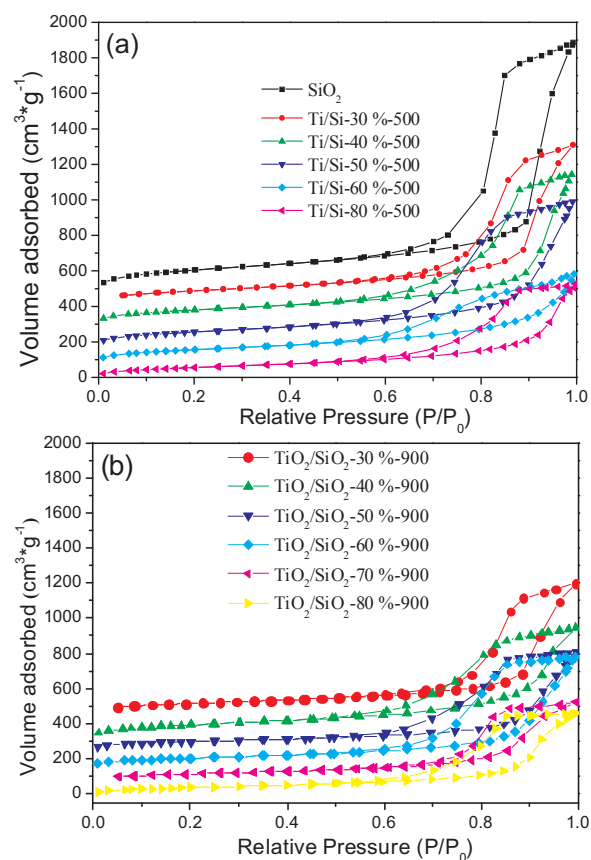


Fig. 4. N_2 adsorption-desorption isotherms of SiO_2 and $\text{TiO}_2/\text{SiO}_2$ composites with various TiO_2 concentrations calcined at 500 °C (a) and 900 °C (b).

surface area were about 16% and 50% for the Ti/Si-30% and Ti/Si-80%, respectively. Such great decrease of surface area for the high concentration of TiO_2 sample was owing to the serious aggregation of the TiO_2 grains loaded on the out surface of the pore channels of silica foam. The direct evidence of the anatase TiO_2 -QDs nanocrystals located inside the pore channels of SiO_2 foams was also obtained from the TEM and HRTEM results (Fig. 5). As shown in Fig. 5a, the meso-cellular pore wall the SiO_2 foam was uniformly anchored with lots of black spots, corresponding to the ultrafine TiO_2 -QDs, for the sample of Ti/Si-50%-900. These QDs were highly embedded in these pore channels of the SiO_2 foam with a random orientation. The HRTEM image (Fig. 5b) further revealed that the as-formed TiO_2 -QDS on the SiO_2 foam were well crystallized, as evidenced by well-defined lattice fringes. The lattice fringes at 0.357 nm match planes of d-spacing (d101, 3.514 Å) of anatase TiO_2 . The TiO_2 crystals size measured in the HRTEM images for Ti/Si-60%-900 was at the range of 5–8 nm (quantum dots size) in good agreement with the crystal domain size measured by XRD. For better comparison, the typical mesoporous silica (SBA-15) was also utilized to load the TiO_2 species. As shown in Fig. 5c, it was also noted that TiO_2 nanocrystals were accumulated outside of the SBA-15 channels even the molar ratio of Ti/Si is lower as 40%. The accumulation of TiO_2 outside of the pore channels may be ascribed to the small pore size and 2D dimension of SBA-15. These results suggested that the presence of the large pores in the 3D SiO_2 foams played an important role in enhancing the loaded amount of TiO_2 nanocrystals anchored in the pore channels of SiO_2 supporters while keeping its high dispersity, thus, the as-obtained TiO_2 -QDs could be well inhibited from aggregation and exposed with more surface to trap light during the photocatalytic reactions.

For further evidencing the strong interaction between the TiO_2 -QDS and the surface of the SiO_2 foams, both FT-IR and XPS characterizations were performed. Fig. 6a shows the FT-IR spectra of the TiO_2 -DQs/ SiO_2

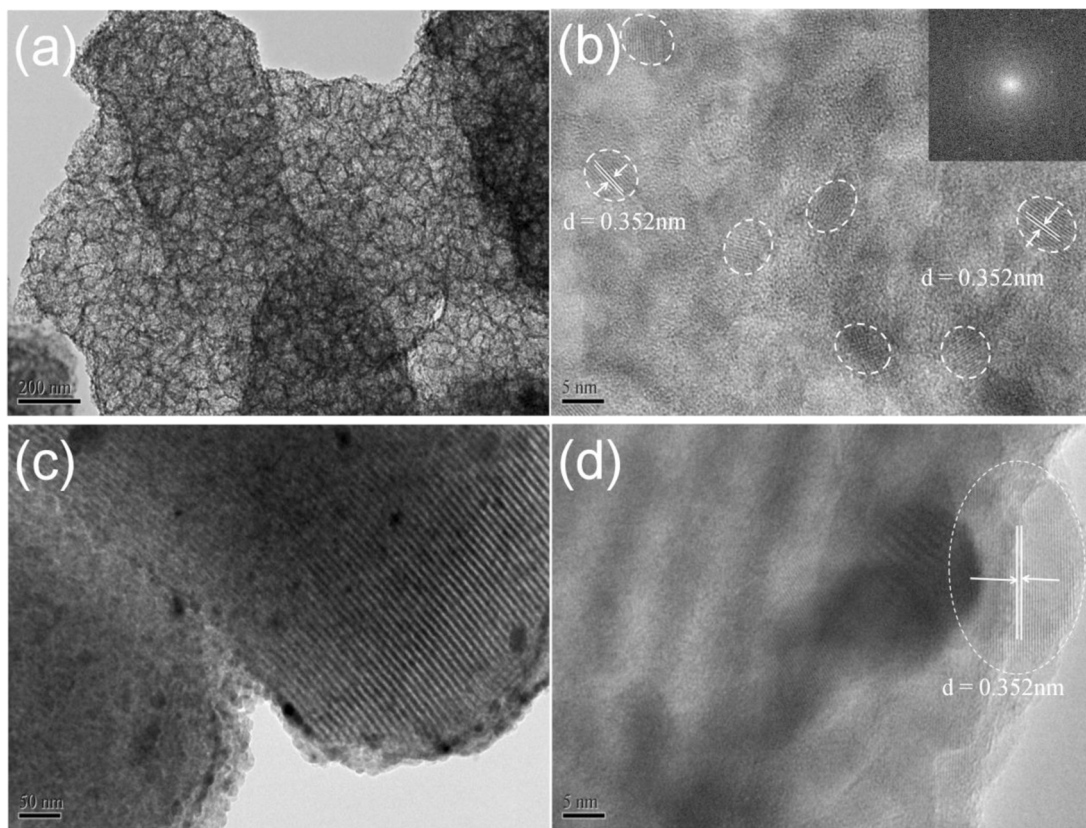


Fig. 5. TEM images and HRTEM images of $\text{TiO}_2/\text{SiO}_2$ -50%-900 (a) and (b), $\text{TiO}_2/\text{SBA-15}$ -40%-900 (c) and (d), and TiO_2 crystals marked by white cycles (Inset is the corresponding FFT pattern).

samples calcined at 500 °C. For the all spectra, the bands at about 3423 and 1627 cm^{-1} can be attributed to the stretching vibration of hydroxyl and water, respectively [53]. It has been reported that adsorbed water, which is probably due to humid KBr and incorporated humidity in the process of sample preparation, has two bands around 3400 and 1630 cm^{-1} [54,55], while the Ti-OH bonds presented three bands around 3563, 3172 and 1600 cm^{-1} [56]. A clear broad and gradually increase band at the range of 400–600 cm^{-1} can also be observed, which can be assigned to the vibration of the Ti-O-Ti moiety of the titanium dioxide network, suggesting the formation of TiO_2 . The other three bands (806, 1087, and 1383 cm^{-1}) were associated with the Si—O bonding [57]. In addition to these peaks, theoretically, a band at 960 cm^{-1} was generally attributed to the overlapping of vibrations of Ti—O—Si and Si—OH bonds [58,59]. Such bands at 960 cm^{-1} was clearly observed for all of samples, suggesting the formation of Ti—O—Si bonds for all the as-obtained $\text{TiO}_2/\text{SiO}_2$ samples. Interestingly, the increase rate of the intensity at 960 cm^{-1} was very low at the low Ti/Si molar ratio (30–50%). XPS was also used to investigate the surface chemical sate of the O1s of silica before and after loading TiO_2 -QDs. From Fig. 6b, it was observed that pure SiO_2 foam possessed a typical O1s peak at 532.8 eV of silica [60], and nearly no obvious typical O1s peak (530.0 eV) [12], ascribed to the lattice oxygen in anatase TiO_2 , was found after loading TiO_2 -QDs with a Ti/Si molar ratio below 50%. This could suggest that nearly all the TiO_2 -QDs were highly dispersed in the pore channels of the silica foam. Further increasing the Ti/Si molar ratio over 60% resulted in a significant increase of the O1s peak at 530.0 eV. This was attributed to the excess TiO_2 species formed on the outer surface of the silica foam, thus, more signals from the lattice oxygen in TiO_2 were trapped. As shown in Fig. 6b, the O1s peak at 531.4 eV was ascribed to the hydroxyl groups. Based on the area integral of the two peaks correspond to the Ti—O—Ti and surface hydroxyl groups, the ratios of $\text{O}_{\text{OH}}/\text{O}_T$ ($\text{O}_T = \text{O}_{\text{OH}} + \text{O}_{\text{Ti-O-Ti}}$) of the as-

obtained samples were calculated [12]. As shown in Table S1, the ratios of $\text{O}_{\text{OH}}/\text{O}_T$ in TiO_2 -QDs/ SiO_2 foam samples were about 48.1% (Ti/Si = 30%), 45.7% (Ti/Si = 40%), 44.3% (Ti/Si = 50%), 37.5% (Ti/Si = 60%), 15.5% (Ti/Si = 80%) and 6.4% (pure TiO_2), respectively. It was noted that low ratio of $\text{O}_{\text{OH}}/\text{O}_T$ would result in a serious aggregation of TiO_2 QDs to the case of Ti/Si=80%-500 (see Fig. S1). These results demonstrated that surface hydroxyl groups could affect the aggregation process of TiO_2 QDs [61]. Meanwhile, the binding energy of $\text{Ti}2\text{p}_{3/2}$ (Fig. 6c) in the composite of TiO_2 -QDs/ SiO_2 was positively shifted upon decreasing the Ti/Si molar ratio. Among all these samples, Ti/Si-30%-500 exhibited the highest $\text{Ti}2\text{p}$ binding energy (258.8 eV). Such positive shift also indicated the strong interaction between the TiO_2 -QDs and the pore wall of SiO_2 foam through the Ti—O—Si bonds. Based on both the FT-IR and XPS results, it was reasonable that the as-formed TiO_2 -QDs were strongly anchored on the inner surface of the SiO_2 foams with a high dispersion and intense interaction.

For better understanding the electronic states of these TiO_2 -QDs/ SiO_2 samples, UV-vis diffuse reflectance spectroscopy (DRS) was performed. As shown in Fig. 7a, TiO_2 -500 exhibited an adsorption edge at 398 nm, however, the edge position was greatly blue shifted to 373 nm upon loading TiO_2 -QDs with a Ti/Si molar ratio of 30%. From Fig. 7b, the optical band energies of both the TiO_2 -500 and Ti/Si-30%-500 were estimated to be about 3.12 eV and 3.32 eV, respectively, from the $(\text{ahv})^{1/2}$ versus photon energy plots [62]. The blue shift with broadened band gaps for the TiO_2 species on the SiO_2 foam was owing to the ultrafine crystal size of the TiO_2 -QDs anchored on SiO_2 (quantum size effect) [63,64]. It was well-known that quantum size effects (QSE) were usually observed for semiconductor crystal grains in a ultrafine nanoscale (1–10 nm). If the size of the semiconductor crystals was nearly same as the de Broglie wavelength of the charge carriers in semiconductors, the anomalies will arise and both electron and hole generated in quantum dots will be confined in a potential well of small

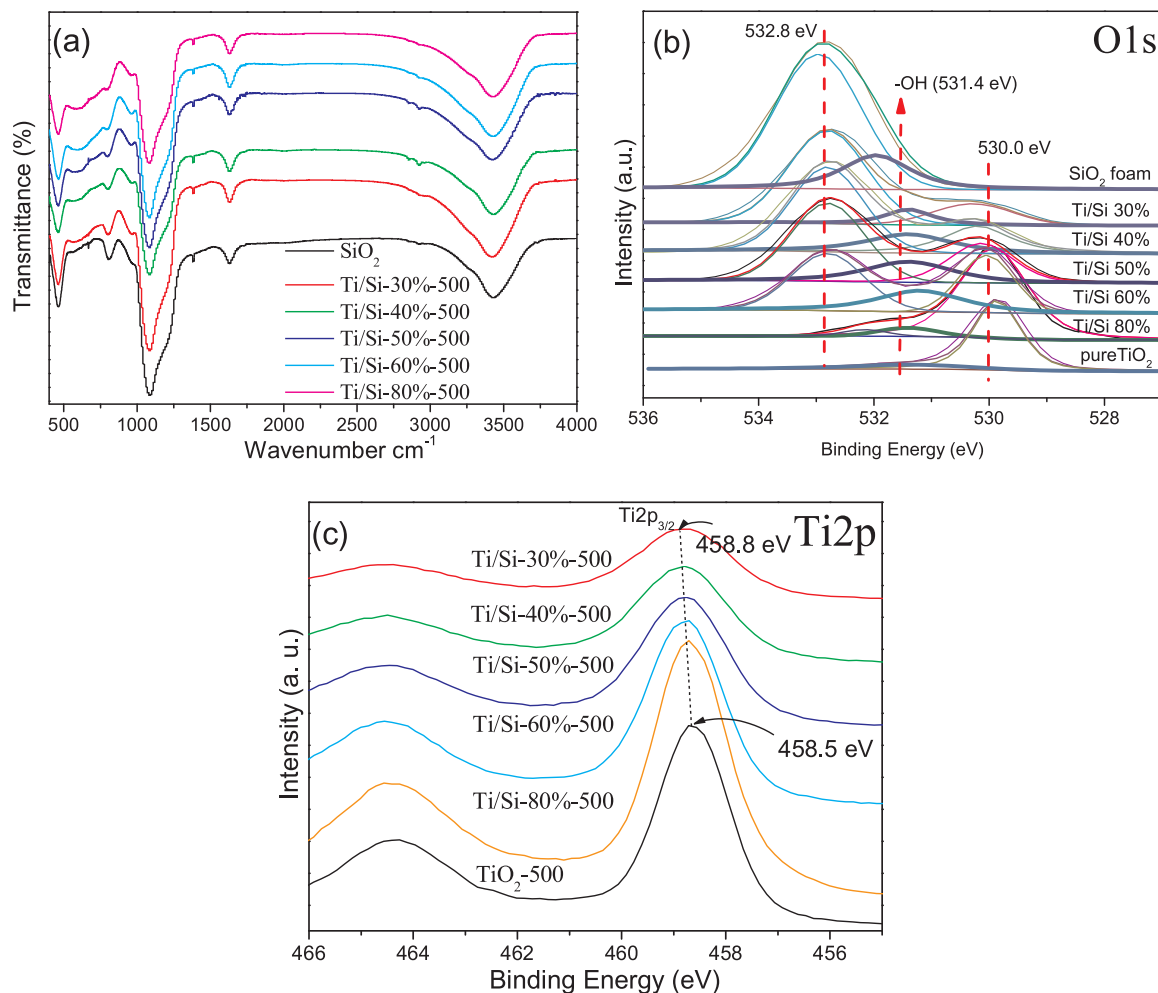


Fig. 6. FT-IR spectra (a) and XPS spectra (b, c) of the as-formed samples.

geometrical dimensions. Thus, the confinement in several nanometers will produce a quantization of discrete electronic states with the formation of an increased band gap of semiconductor [64]. It was also observed that the UV light ($\lambda < 330 \text{ nm}$) absorption capability of the TiO_2 was significantly enhanced upon being loaded on SiO_2 foam. This may be also ascribed to the QSE. These results confirmed that TiO_2 -QDs were well formed limited in the pore channels of the 3D SiO_2 foams, and the proposed route with the aid of SiO_2 foam can also effectively prohibit the aggregation of the TiO_2 crystals and enhancing the light-

trapping ability owing to QSE.

For clarifying the photocatalytic performance of the as-obtained samples, the photocatalytic evolution of H_2 was utilized as probe reaction under UV-light ($\lambda = 365 \text{ nm}$) irradiation. All the H_2 evolution rates (HER) were converted into a standard value as unit mass of TiO_2 species as shown in Fig. 8a. To the case of the samples calcined at 500 °C, it was found that the pure TiO_2 possessed a HER of $6934.0 \mu\text{mol g}^{-1} \text{ h}^{-1}$. The TiO_2 -QDs loaded on the SiO_2 foam exhibited a lower H_2 evolution rate when the Ti/Si molar ratio was below 40%.

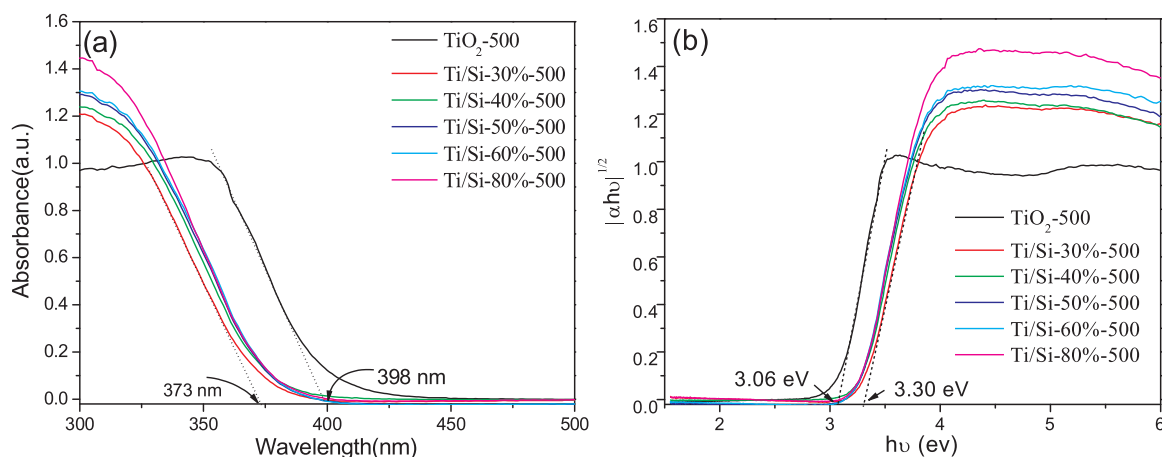


Fig. 7. Diffused reflectance UV-vis spectra of pure TiO_2 and TiO_2 -QDs/ SiO_2 with various of Ti/Si molar ratio calcined at 500 °C.

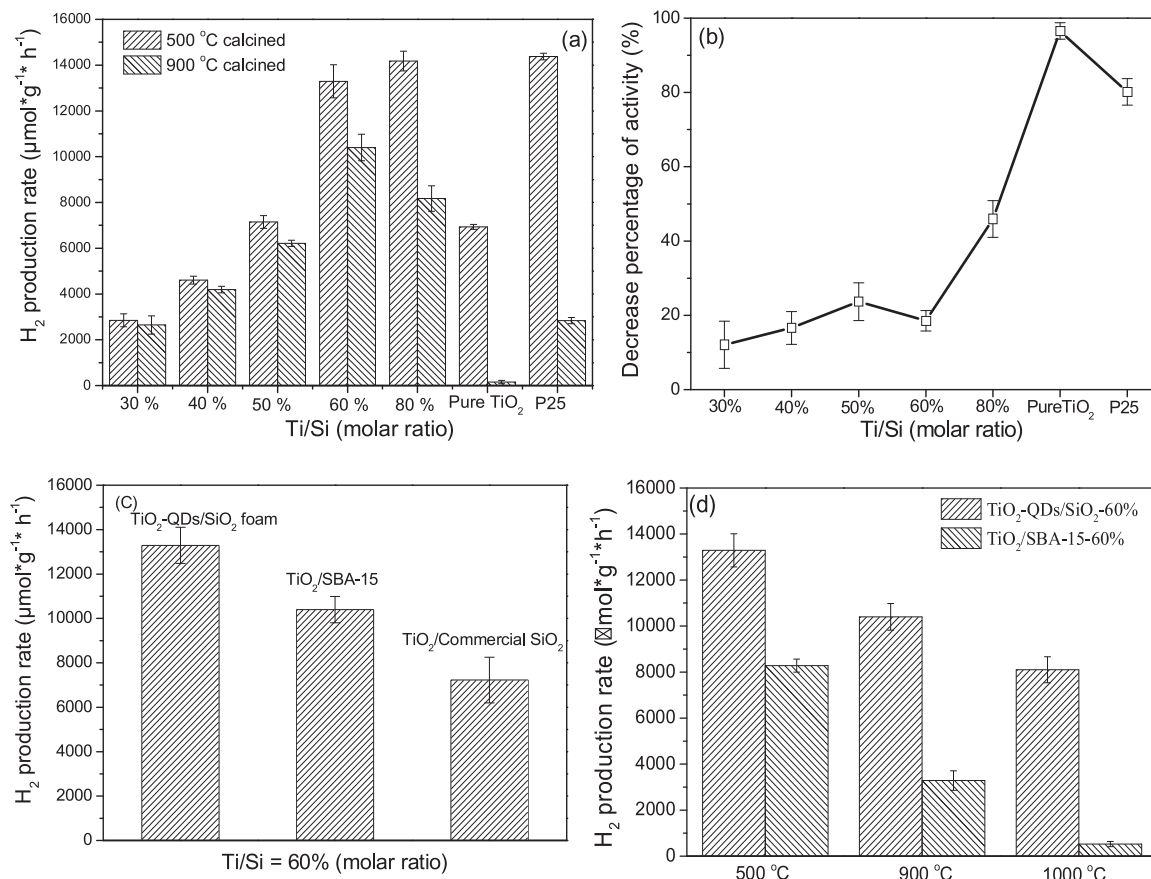


Fig. 8. (a) The photocatalytic H₂ evolution rate of the TiO₂-QDs/SiO₂, pure TiO₂ and commercially available TiO₂ (P25) calcined at 500 and 900 °C; (b) the decrease percentage of the H₂ evolution activity from 500 to 900 °C; (c) The H₂ evolution rate of the TiO₂-QDs/SiO₂, TiO₂/SBA-15 and TiO₂/commercial SiO₂ with a Ti/Si molar ratio of 60% under 500 °C calcination; (d) The comparison of TiO₂-QDs/SiO₂-60% and TiO₂/SBA-15-60% calcined at different temperature for H₂ evolution.

This could be ascribed to the coverage of the active sites owing to the SiO₂ foam. As known, nearly all of the TiO₂-QDs were located in the pore channels of SiO₂ foam, thus, the exposed surface for trapping light was very limited. Upon further increasing the Ti/Si molar ratio over 50%, the HER was greatly enhanced and the sample of Ti/Si-80%-500 exhibited a HER of 14178 μmol g⁻¹ h⁻¹. Nevertheless, it should be noticed that the pure TiO₂ nearly cannot possess an obvious HER value upon being calcined at 900 °C. Such significant decrease of HER may suffer from the low surface area owing to the serious aggregation of TiO₂ nanocrystals under high temperature treatment. The photocatalytic HER performance of the commercial available TiO₂ (P25) was also tested as a reference. As the results indicated, though the H₂ revolution rate of P25 higher than that of the TiO₂-QDs/SiO₂ samples calcined at 500 °C. A significant decrease (about 80%) of HER value was observed for P25 after being calcined at 900 °C. Fortunately, the HER values of all the SiO₂ foam protected TiO₂-QDs were well maintained though a slight decrease was observed. Among them, the sample of Ti/Si-60%-900 exhibited the highest HER (10399 μmol g⁻¹ h⁻¹) with a quantum efficiency of 17.8% under UV light irradiation ($\lambda = 365$ nm). Such excellent thermal stability of these TiO₂-QDs can be attributed to the protection effect of SiO₂ foam. It can effectively inhibit the aggregation of TiO₂ nanocrystals, meanwhile, these QDs can be crystallized into nano grains with high crystallinity confined in the pore channels of SiO₂ foams. These results have been proved by XRD and TEM results. For clearly demonstrating the promotion effect silica foam, the decrease percentage of the HER for the as-obtained samples (calcined at 500 and 900 °C) was also calculated as shown in Fig. 8b. It was noted that the decrease percentage can be maintained to be about 10% when the Ti/Si molar ratio was below 60%. Such value was significantly enhanced to over 40% in the presence of high Ti/Si molar

ratio (> 80%). These results suggested that SiO₂ foam can well maintain the TiO₂-QDs under high temperature calcination when the Ti/Si molar ratio was below 60%. Overloaded TiO₂-QDs will accumulate on the out surface of silica channels. The channel confined effect cannot work for enhancing the thermal stability of these TiO₂-QDs.

For comparison, SBA-15 and commercial SiO₂ nanospheres were also utilized as different supports for loading TiO₂ species under various temperature calcination with a Ti/Si molar ratio of 60%. The photocatalytic HER activity of these samples with different supports was also evaluated as shown in Fig. 8(c). Owing to the 3D structure of SiO₂ foam, the sample of TiO₂-QDs/SiO₂-60%-500 exhibited the highest HER value. From 500 to 1000 °C, the sample of TiO₂/SBA-15-60% suffered a 93.7% decrease of HER value. Only a 31.2% decrease of HER was observed to the case of TiO₂-QDs/SiO₂-60%. These results implied that the intense interfacial contact and strong interaction between TiO₂ nanoparticles and SiO₂ foams with the larger pore size may play an important role in the enhancement of photocatalytic activity for TiO₂-QDs. Because of the 3D structure of silica foams with larger pore size, nearly all the TiO₂ species were located in the pore channels of silica foams. As illustrated in Fig. 9, these 3D pores in the silica foam will confine these QDs limited in the pore cavity, thus the aggregation of nanocrystals will be effectively inhibited while obtaining high crystallinity at higher temperature calcination. Meanwhile, a short pathway for the electron transfer will be achieved for accelerating the electron transfer from the bulk to the surface of the TiO₂-QDs. For exploring the potential photocatalytic application in environmental treatment, the as-formed TiO₂-QDs/SiO₂ foam samples were utilized to degrade 4-CP (a typical kind of toxic organic molecules). As shown in Fig. 10, the sample of TiO₂-QDs/SiO₂-60%-500 exhibited a higher activity for degrading 4-CP compared with TiO₂/SBA-15-60%-500. After 180 min of

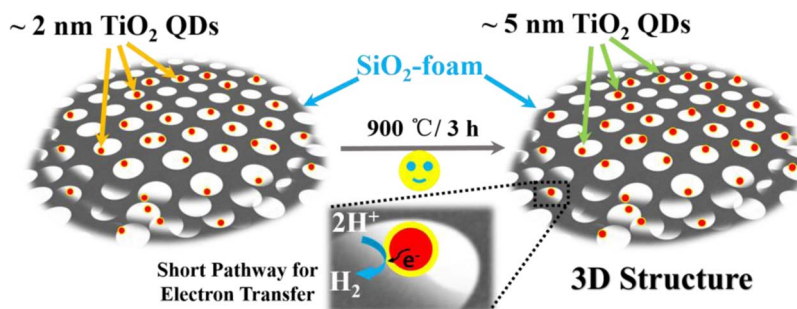


Fig. 9. The illustration of silica foam for enhancing the thermal stability of TiO₂-QDs with short electrons transfer pathway.

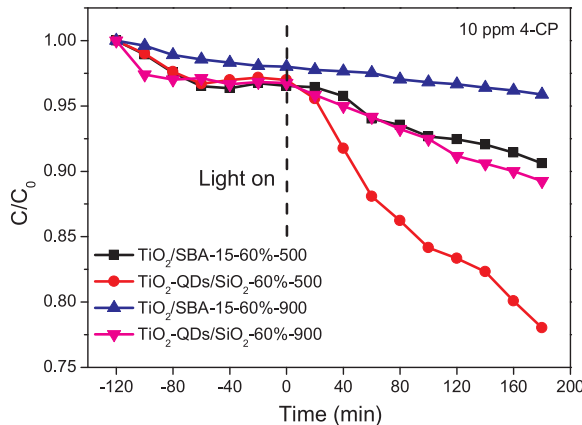


Fig. 10. The photocatalytic degradation of 4-CP for TiO₂/SBA-15 and TiO₂-QDs/SiO₂ foam with the same Ti/Si molar ratio (60%) under 300 W Xe lamp irradiation.

reaction, the former obtained a 25% removal rate of 4-CP, while the latter just possessed a 10% removal rate of 4-CP. Moreover, the photocatalytic degradation performance was significantly decreased when the sample of TiO₂/SBA-15-60% was calcined 900 °C. Nevertheless, the sample of TiO₂-QD/SiO₂-60%-900 still maintained an obvious degradation rate for treating 4-CP. All the above results indicated that the as-obtained TiO₂-QD/SiO₂ foam sample possessed strong photocatalytic activity for both H₂ evolution and degradation of toxic pollutants with high thermal stability.

4. Conclusions

In summary, a facile strategy based on the internal hydrolysis of Ti-alkoxide in the SiO₂ foams with 3D pore channels was explored to the fabrication of highly active and thermally stable TiO₂-QDs embedded in SiO₂ foams. These TiO₂-QDs were strongly anchored in the cavities of the SiO₂ foam. Such cavity-confine effect resulted from the SiO₂ foam effectively inhibited the TiO₂ phase transformation from anatase to rutile and the aggregation of the TiO₂ nanocrystals to larger particles, allowing the as-formed TiO₂-QDs to possess large surface area and high crystallinity during high temperature calcination. The 3D large pores of the silica foams can be maintained unblocked even after being loaded TiO₂-QDs with a high Ti/Si molar ratio up to 60%, thus more light can reach the photoactive sites of TiO₂. Such anatase TiO₂-QDs anchored in the SiO₂ foam could be well maintained with an ultrafine crystal size (6.3 nm, molar ratio of Ti/Si = 60%, 900 °C) even after high temperature (up to 1000 °C) calcination in air, suggesting a high thermal stability. The sample of TiO₂-QDs/SiO₂ photocatalysts (molar ratio of Ti/Si = 60%, 900 °C) still exhibited a high H₂ evolution rate (HER, 10399 μmol/g·h) for reducing water with a quantum efficiency of 17.8% under UV light irradiation ($\lambda = 365$ nm). Such proposed route offered an effective platform for fabricating highly active TiO₂ quantum dots with high thermal stability, greatly prolonging its recyclability

in other applications, including solar cell, high temperature catalysis, and etc.

Acknowledgments

This work was supported by the National Natural Science Foundation of China (21477079, 21677099), Shanghai Government Project (15QA1403300), Yunnan Applied Basic Research Project of Province (C0120150543), Key Projects of Yunnan Provincial Department of Education (2015Z183, 2016ZZX207) and the International Joint Laboratory on Resource Chemistry (No. IJLRC).

Appendix A. Supplementary data

Supplementary material related to this article can be found, in the online version, at doi:<https://doi.org/10.1016/j.apcatb.2018.02.022>.

References

- [1] R. Künneth, G. Twardzik, G. Emig, H. Kisch, J. Photochem. Photobiol. A Chem. 76 (1993) 209–215.
- [2] H. Kisch, Angew. Chem. Int. Ed. 52 (2013) 812–847.
- [3] L.F. Li, X.L. Zhao, D.L. Pan, G.S. Li, Chin. J. Catal. 38 (2017) 2132–2140.
- [4] S.N. Xiao, P.J. Liu, W. Zhu, G.S. Li, D.Q. Zhang, H.X. Li, Nano Lett. 15 (2015) 4853–4858.
- [5] Z.C. Lian, W.C. Wang, S.N. Xiao, X. Li, Y.Y. Cui, D.Q. Zhang, G.S. Li, H.X. Li, Sci. Rep. 5 (2015) 10461.
- [6] S.L. Wang, S.H. Lin, D.Q. Zhang, G.S. Li, M.K.H. Leung, Appl. Catal. B Environ. 215 (2017) 85–92.
- [7] G.S. Li, Z.C. Lian, W.C. Wang, D.Q. Zhang, H.X. Li, Nano Energy 19 (2016) 446–454.
- [8] Z.C. Lian, W.C. Wang, G.S. Li, F.H. Tian, K.S. Schanze, H.X. Li, ACS Appl. Mater. Interfaces 9 (2017) 16960–16967.
- [9] Z. Zhang, C. Wang, R. Zakaria, J. Ying, J. Phys. Chem. B 102 (1998) 10871–10878.
- [10] A. Deshpande, N.M. Gupta, Int. J. Hydrogen Energy 35 (2010) 3287–3296.
- [11] S. Wang, S. Lin, D. Zhang, G. Li, M.K.H. Leung, Appl. Catal. B Environ. 215 (2017) 85–92.
- [12] G.S. Li, D.Q. Zhang, J.C. Yu, Phys. Chem. Chem. Phys. 11 (2009) 3775–3782.
- [13] D. Zhang, G. Li, J.C. Yu, Cryst. Growth Des. 9 (2009) 2812–2815.
- [14] J. Liu, X. Yang, K. Wang, X. He, Q. Wang, J. Huang, Y. Liu, ACS Nano 6 (2012) 4973.
- [15] S.V. Vaidya, A. Couzis, C. Maldarelli, Langmuir 31 (2015) 3167–3179.
- [16] J. Yan, P.D. McNaughton, Z. Wang, N. Hodson, M. Chen, Z. Cui, P. O'Brien, B.R. Saunders, RSC Adv. 5 (2015) 95512–95522.
- [17] S. Zhang, Y. Jiang, C.S. Chen, J. Spurgin, K.A. Schwehr, A. Quigg, W.C. Chin, P.H. Santschi, Environ. Sci. Technol. 46 (2012) 8764–8772.
- [18] X. Zhang, S. Lin, J. Liao, N. Pan, D. Li, X. Cao, J. Li, Electrochim. Acta 108 (2013) 296–303.
- [19] F. Hetsch, X. Xu, H. Wang, S.V. Kershaw, A.L. Rogach, J. Phys. Chem. Lett. 2 (2011) 1879–1887.
- [20] T.R. Sathe, A. Agrawal, S. Nie, Anal. Chem. 78 (2006) 5627.
- [21] N. Hao, L. Jiang, J. Qian, K. Wang, J. Electroanal. Chem. 781 (2016) 332–338.
- [22] J. Leśnicki, B. Szafrań, Phys. Rev. B 95 (2017).
- [23] S. Mohapatra, S. Sahu, S. Nayak, S.K. Ghosh, Langmuir 31 (2015) 8111–8120.
- [24] X. Li, X. Yang, L. Yuwen, W. Yang, L. Weng, Z. Teng, L. Wang, Biomaterials 96 (2016) 24–32.
- [25] L. Stanca, A.I. Serban, C. Grigoriu, A. Dinischiotu, Febs J. 280 (2013) 226.
- [26] K.M. Tsoi, Q. Dai, B.A. Alman, W.C. Chan, Acc. Chem. Res. 46 (2013) 662.
- [27] Y. Zhu, L. Zhang, C. Gao, L. Cao, J. Mater. Sci. 35 (2000) 4049–4054.
- [28] J.C. Yu, J. Yu, J. Zhao, Appl. Catal. B Environ. 36 (2002) 31–43.
- [29] P. Cheng, M. Zheng, Y. Jin, Q. Huang, M. Gu, Mater. Lett. 57 (2003) 2989–2994.
- [30] C. Minero, F. Catocco, E. Pelizzetti, Langmuir 8 (1992) 481–486.

- [31] A.S. Besov, A.V. Vorontsov, V.N. Parmon, *Appl. Catal. B Environ.* 89 (2009) 602–612.
- [32] P.D. Cozzoli, A. Kornowski, H. Weller, *J. Am. Chem. Soc.* 125 (2003) 14539.
- [33] J. Yang, J. Zhang, L. Zhu, S. Chen, Y. Zhang, Y. Tang, Y. Zhu, Y. Li, J. Hazard. Mater. 137 (2006) 952–958.
- [34] X. Li, W. Zheng, H. Pan, Y. Yu, L. Chen, P. Wu, *J. Catal.* 300 (2013) 9–19.
- [35] P. Schmidt-Winkel, W.W. Lukens, D. Zhao, P. Yang, B.F. Chmelka, G.D. Stucky, *J. Am. Chem. Soc.* 121 (1999) 254–255.
- [36] H.G. Yang, C.H. Sun, S.Z. Qiao, J. Zou, G. Liu, S.C. Smith, H.M. Cheng, G.Q. Lu, *Nature* 453 (2008) 638–641.
- [37] J.S. Chen, Y.L. Tan, C.M. Li, Y.L. Cheah, D. Luan, S. Madhavi, F.Y. Boey, L.A. Archer, X.W. Lou, *J. Am. Chem. Soc.* 132 (2010) 6124.
- [38] S.C. Pillai, P. Periyat, R. George, D.E. McCormack, M.K. Seery, H. Hayden, J. Colreavy, D. Corr, S.J. Hinder, *J. Phys. Chem. C* 111 (2007) 1605–1611.
- [39] H.B. Wu, H.H. Hng, X.W. Lou, *Adv. Mater.* 24 (2012) 2567–2571.
- [40] N. Doss, P. Bernhardt, T. Romero, R. Masson, V. Keller, N. Keller, *Appl. Catal. B Environ.* 154–155 (2014) 301–308.
- [41] T. Hao, G. Cheng, H. Ke, Y. Zhu, Y. Fu, *RSC Adv.* 4 (2014) 21548–21552.
- [42] J. Fan, C. Yu, L. Wang, B. Tu, D. Zhao, Y. Sakamoto, O. Terasaki, *J. Am. Chem. Soc.* 123 (2001) 12113–12114.
- [43] K. Sing, *Pure Appl. Chem.* 57 (1985) 603–619.
- [44] M. Kruk, M. Jaroniec, *Chem. Mater.* 13 (2001) 3169–3183.
- [45] S.Y. Chai, Y.J. Kim, M.H. Jung, A.K. Chakraborty, D. Jung, W.I. Lee, *J. Catal.* 262 (2009) 144–149.
- [46] Q. Huo, R. Leon, P.M. Petroff, G.D. Stucky, *Science* 268 (1995) 1324.
- [47] W.J. Stevens, K. Lebeau, M. Mertens, T.G. Van, P. Cool, E.F. Vansant, *J. Phys. Chem. B* 110 (2006) 9183–9187.
- [48] M.V. Landau, L. Vradman, X. Wang, L. Titelman, *Microporous Mesoporous Mater.* 78 (2005) 117–129.
- [49] E. Beyers, P. Cool, E.F. Vansant, *Microporous Mesoporous Mater.* 99 (2007) 112–117.
- [50] F. Chiker, J.P. Nogier, F. Launay, J.L. Bonardet, *Appl. Catal. A* 243 (2003) 309–321.
- [51] H.C. Yang, H.Y. Lin, Y.S. Chien, J.C.S. Wu, H.H. Wu, *Catal. Lett.* 131 (2009) 381–387.
- [52] M. Guidotti, N. Ravasio, R. Psaro, G. Ferraris, G. Moretti, *J. Catal.* 214 (2003) 242–250.
- [53] Y. Suda, T. Morimoto, *Langmuir* 3 (1987) 786–788.
- [54] K. Tanaka, J.M. White, *J. Phys. Chem.* 86 (1982) 4708–4714.
- [55] E. Sanchez, T. Lopez, R. Gomez, A. Bokhimi, O. Morales, Novaro, *J. Solid State Chem.* 122 (1996) 309–314.
- [56] G.A. Eimer, S.G. Casuscelli, G.E. Ghione, M.E. Crivello, E.R. Herrero, *Appl. Catal. A* 298 (2006) 232–242.
- [57] N. Benito, C. Palacio, *Appl. Surf. Sci.* 301 (2014) 436–441.
- [58] P. Wu, T. Tatsumi, T. Komatsu, T. Yashima, *Chem. Mater.* 14 (2002) 1657–1664.
- [59] C. Hess, G. Tzolova-Müller, R. Herbert, *J. Phys. Chem. C* 111 (2007) 9471–9479.
- [60] K.A. Dunphy Guzman, M.P. Finnegan, J.F. Banfield, *Environ. Sci. Technol.* 40 (2006) 7688–7693.
- [61] X. Peng, G.W. Meng, J. Zhang, L. Zhao, X. Wang, Y. Wang, L. Zhang, *J. Phys. D* 34 (2001) 3224–3228.
- [62] G. Liu, H.G. Yang, J. Pan, Y. Yang, G. Lu, H. Cheng, *Chem. Rev.* 114 (2014) 9559–9612.
- [63] A. Linsebigler, G. Lu, J. Yates, *Chem. Rev.* 95 (1995) 735–758.
- [64] G.S. Li, D.Q. Zhang, J.C. Yu, *Chem. Mater.* 39 (2008) 3983–3992.